Analyzing vegetation effects on snow depth variability in Alaska's boreal forests with airborne lidar

Lora D. May[1], Svetlana Stuefer[1], Scott Goddard[2], Christopher Larsen[3]

[1]Department of Civil, Geological and Environmental Engineering, Water and Environmental Research Center, University of Alaska Fairbanks, Fairbanks, Alaska, 99775, USA
[2]Department of Mathematics and Statistics, University of Alaska Fairbanks, Fairbanks, Alaska, 99775, USA
[3]Geophysical Institute, University of Alaska Fairbanks, Fairbanks, Alaska, 99775, USA

Correspondence to: Lora D. May (ldmay3@alaska.edu)

Abstract. Lidar-derived snow depth and canopy height maps were used to analyze snow depth spatial variability at a boreal forest site in Alaska. High resolution (0.5 m) airborne lidar data were acquired during NASA's SnowEx Alaska field campaigns during peak snow-on accumulation (March 2022) and snow-off (May 2022). The impact of canopy height on snow distribution was studied at the Caribou Poker Creeks Research Watershed, located north-east of Fairbanks, Alaska, U.S. Ground-based snow depth measurements were collected concurrently with the March snow-on lidar survey and were compared to collocated lidar-derived snow depths. The comparison between ground-based and lidar-derived snow depths produced a bias of 2.0 cm and a root mean square error (RMSE) of 12.0 cm. The lidar snow depth map showed a mean snow depth of $\overline{HS}$ = 98 cm and SD = 15 cm for the study site. The influence of vegetation on end-of-winter snow depth distribution was analyzed using three canopy height classes: 1) forest, 2) shrub and short stature trees (SSS), and 3) treeless. Results showed a statistically significant difference in median snow depths across canopy height classes, with the largest significant difference between forest and treeless (12–14 cm) and between forest and SSS (8–14 cm). This difference in snow depths is equivalent to an SWE range of 0.02–0.03 m. This study provides insights into the spatial variability of snow depths in Alaska's boreal forests by using ground-based measurements to evaluate the accuracy of lidar to estimate snow depths in a boreal forest ecosystem. The results of this research can be used to assist water and resource managers in determining best practices for estimating snow depth and its spatial variability in the boreal forest of Alaska.

1 Introduction

Snow plays a significant role in hydrologic, atmospheric, and ecological processes globally. Snow cover impacts the thermal regime of the soil, water and energy balances, land use decisions, winter recreation, and the timing and volume of spring runoff (Barnett et al., 2005; Boelman et al., 2019; Chapin et al., 2000, 2005). In the boreal forest seasonal snowpack and its melting dominate annual hydrological and climatic patterns (Barnett et al., 2004; Kane and Yang, 2004; Kozii et al., 2017). The snowpack accumulates from the fall through the following spring with few melt or runoff events. The spring snowmelt is often

the major hydrological event each year, and usually correlates to the peak discharge of the season (Kane and Yang, 2004; Kozii et al., 2017; Tennant et al., 2017).

In boreal forest regions, the spatial and temporal variability of snow depth (HS) can be significant due to static controls such as land cover, topography, soil, and permafrost (Cho et al., 2021; Pastick et al., 2015; Woo, 2012) and to dynamic processes
35 including canopy-snow interactions (Hojatimalekshah et al., 2021; Kozii et al., 2017; Uhlmann et al., 2018), wind distribution (Homan and Kane, 2015; Liston and Sturm, 1998), long and short wave radiation (Lundquist et al., 2013), and solid and liquid precipitation trends (Bolton et al., 2004; Brown and Goodison, 1996; Kane and Yang, 2004; Lader et al., 2020). Boreal forest snow is classified as cold with thin to moderate (0.3–1.3 m) snow depths and low-density layers (Sturm and Liston, 2021). The low density is due to the extensive depth hoar (occupying 2/3 to virtually all the snow cover), and little to no melt events
40 during the winter season. New and recent snow layers at the surface of the snow retain their basic snow crystal structures for days due to the cold air temperatures, relatively low amounts of precipitation and the absence of wind (Sturm and Liston, 2021).

The boreal forest is one of the world's largest forest biomes making up approximately 30 % of the world's forested regions (Askne et al., 2017). In the Northern Hemisphere, 20% of the seasonal snow cover occurs within forested regions (Güntner et
45 al., 2007). Forests canopies modify snow accumulation, ablation rates and overall snow storage by intercepting snowfall (Dickerson-Lange et al., 2021; Lundquist et al., 2013; Storck et al., 2002; Uhlmann et al., 2018). Intercepted snow can account for as much as 40–60% of annual snowfall in boreal forests (Kozii et al., 2017; Pomeroy et al., 2002). All these processes are strongly controlled by the structure of the forest canopy at small spatial scales that interact to create variable snow distribution patterns (Broxton et al., 2015, 2019; Dickerson-Lange et al., 2021; Mazzotti et al., 2019). In boreal regions land cover is a
50 mixture of spruce, deciduous, and mixed forests, shrublands, and low-lying herbaceous wetlands. Snow depth can be noticeably different across land cover types under the same climatic conditions. Accurately accounting for forest effects on snow storage and distribution will become even more important as forests change due to warming climate conditions, forest disturbances, wildfires, insect infestation, and permafrost degradation (Panda et al., 2010; Smith et al., 2021). In turn, these changing forests impact hydrological regimes, water availability, timing and magnitude of snowmelt runoff, and water
55 resources for land and civilian uses (Dickerson-Lange et al., 2021; Hopkinson et al., 2004; Mazzotti et al., 2019; Webb et al., 2020).

Monitoring forest changes and subsequent snow storage and distribution effects is vitally important to water and resource managers. Remote sensing techniques are advancing our understanding of links between forest snow distribution and canopy structure by providing high resolution spatial data of snow on the ground and the detailed structure of forest canopies at
60 landscape scales and across previously unavailable extends (Harpold et al., 2014; Jacobs et al., 2021; Li et al., 2021). One remote sensing technique, airborne-based light detection and ranging (lidar), has been used for almost two decades to describe snow depths in forests (Hopkinson et al., 2004), and lidar techniques are evolving to better characterize forest properties (land cover, canopy density, height, gaps, etc.) relevant to snow distribution (Li et al., 2021; Mazzotti et al., 2019; Moeser et al., 2016; Tennant et al., 2017; Yang et al., 2018; Zheng et al., 2016). Studies show that, compared to traditional manual

65   measurements, lidar data that provide spatially continuous, high resolution, snow depth maps have greatly advanced the ability
to characterize spatiotemporal variability in snow depth at larger watershed scales (Deems et al., 2013; Hopkinson et al., 2004,
2012; Jacobs et al., 2021; Nolan et al., 2015; Painter et al., 2016; Trujillo et al., 2007) while maintaining a statistically
significant relationship between lidar-derived snow depths and manual field measurements (Douglas and Zhang, 2021;
Harpold et al., 2014; Hopkinson et al., 2004, 2012; Jacobs et al., 2021; Mazzotti et al., 2019; Reutebuch et al., 2003). However,
70   when comparing lidar accuracy between forest and non-forested areas, existing validation studies yield contrasting conclusions
(Harpold et al., 2014). Despite considerable literature on airborne lidar snow depth retrievals in forested environments, little
research has been published on its ability to measure snow depth in boreal forests, and results are varied identifying what
vegetation characteristics are driving snow depth variability in boreal forest ecosystems.

The purpose of this paper is to contribute to limited boreal forest snow remote sensing research by analyzing ground-based
75   snow depth measurements and airborne lidar data to improve snow depth estimation at an Alaska boreal forest site. Two new
airborne lidar-derived data products obtained during the NASA SnowEx Alaska campaigns are used for the analysis. A lidar-
derived snow depth map is compared to ground-based measurements to evaluate the accuracy of lidar to estimate snow depths
in an Alaska boreal forest. A lidar-derived canopy height map is used to evaluate a vegetation metric that quantifies the spatial
variability of snow depths in boreal forests. The results can then be used to educate and assist water and resource managers in
80   the effectiveness of airborne lidar to accurately estimate snow depth and snow water equivalent (SWE) in boreal forests of
Alaska. The utility of the lidar-derived vegetation metric can further enhance understanding of vegetation and snow
interactions while improving snow modeling applications.

2 Study Site and Data

2.1 Study Site

85   The study was conducted in the Caribou Poker Creeks Research Watershed (CPCRW) located approximately 48 km northwest
of Fairbanks, Alaska (Fig.1). CPCRW is a relatively pristine, 104 km^2 basin reserved for meteorologic, hydrologic, and
ecologic research. The site was established in 1987 as part of the National Science Foundation's Long Term Ecological
Research (LTER) Program, and it is one of only two designated forest research facilities in the true boreal forest zone of the
United States (USDA Forest Service Pacific Northwest Research Station, 2023). The watershed spans an elevation of 200–
90   830 m and reports a mean annual air temperature of -3.3 °C and a mean annual precipitation of 625 mm (USDA Natural
Resources Conservation Service, 2023), 40 % of which can be snowfall (Liston and Hiemstra, 2011; USDA Forest Service
Pacific Northwest Research Station, 2023). Approximately 30 % of its area is underlain by continuous and discontinuous
permafrost (Fig. 1) (Bonanza Creek LTER, 2023; Haugen et al., 1982).

Two streams are found within CPCRW, Caribou Creek and Poker Creek. The Caribou Creek watershed is divided into four
95   subbasins (C1, C2, C3, and C4), and the Poker Creek watershed is divided into six subbasins (P1, P2, P3, P4, P5, and P6) (Fig.
1) (Haugen et al., 1982). The drainage pattern of the two streams is dendritic, and stream channels in the subdrainages are

generally steep-walled and narrow, while the main channels are wider, often with alternating pools and riffles (Bredthauer and Hoch, 1979). The two streams converge at the south-central portion of the watershed and then flow into the Chatanika River. The Chatanika joins the Tolovana River, which flows into the Tanana River and on to the Yukon River. The vegetative cover

100   within the watershed consists of deciduous, evergreen and mixed forests, shrublands, and wetlands. South-facing slopes are dominated by well-drained deciduous and mixed forests of aspen (*Populus tremuloides*), poplar (*Populus balsamifera*), birch (*Betula neoalaskana*), and white spruce (*Picea glauca*). The understory consists of patchy alder (*Alnus viridis*) and willow (*Salix spp.*). North-facing slopes are dominated by evergreen forests with black spruce (*Picea mariana*) as the dominant species. Understories contain dwarf shrubs (e.g., *Betula nana, Salix spp., Ledum groenlandicum*), feather moss, and lichen

105   (Bonanza Creek LTER, 2023).
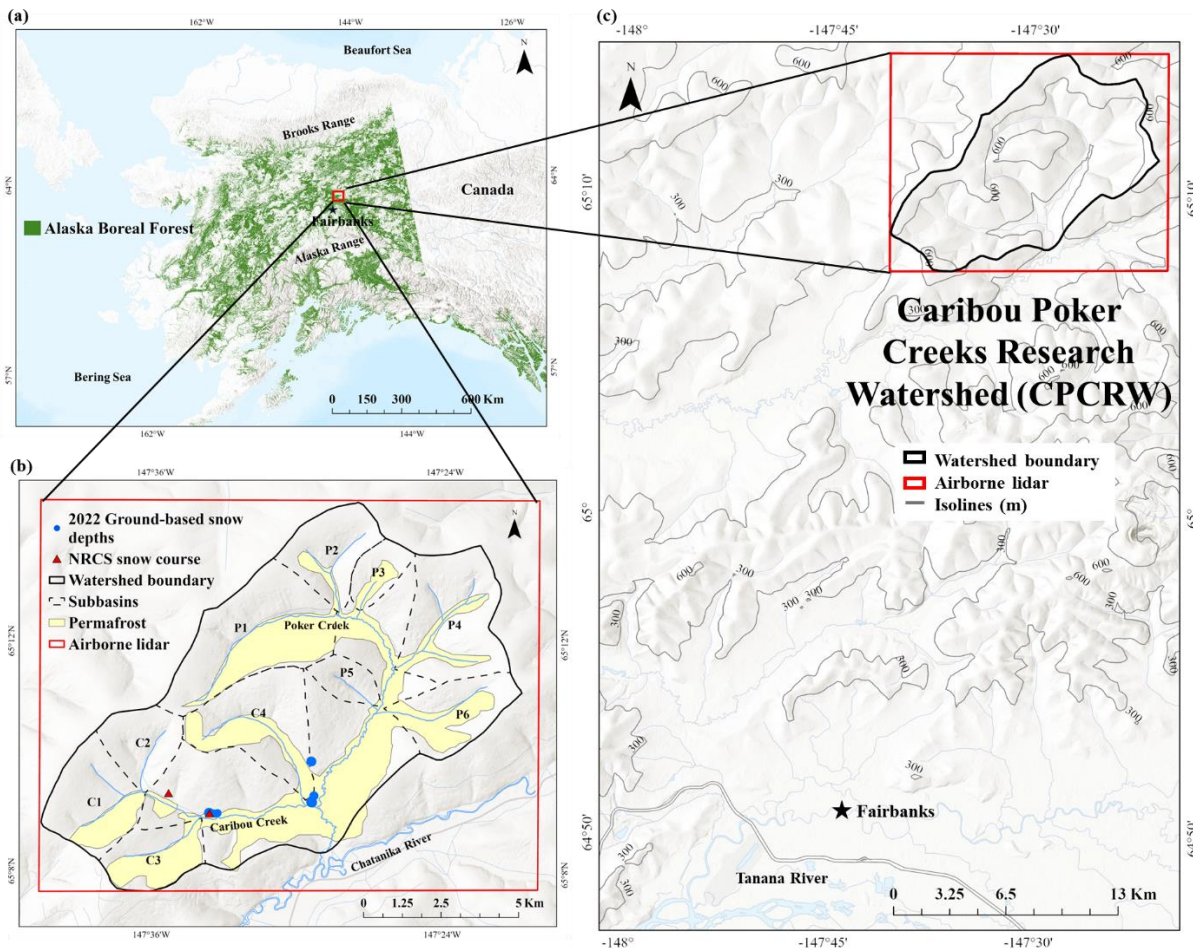
Figure 1: Map of the Alaska boreal forest ecozone (a) and the location of the Caribou Poker Creeks Research Watershed (c). Subbasins of the CPCRW, permafrost areas, the location of ground-based snow depth measurements taken on 11 March 2022, and
110   **the coverage of the lidar flight flown on 11 March 2022, are shown in map (b). Base map source: ESRI.**

2.2 Data

2.2.1 Ground-Based Snow Depths

Ground-based snow depths were obtained from snow measurements conducted in the CPCRW on 11 March 2022 (May et al., 2024), during the planning phase for the NASA SnowEx Alaska campaigns. SnowEx was a multi-year program initiated and
115 funded by the NASA Terrestrial Hydrology Program. SnowEx Alaska aims to ask: "How well we can characterize the spatial variability of snow depth and density needed for accurate SWE estimates in the boreal forest by measuring snow depth, density, and vegetation characteristics" supported by field work and various remote sensing technologies (Vuyovich et al., 2024)? In 2022 and 2023, the NASA SnowEx campaigns were focused on tundra and boreal forest regions of Alaska.

A total of 2,114 ground-based snow depth measurements were collected in a spiral pattern, approximately 1 m apart, with a
120 GPS-enabled snow depth measurement device called a magnaprobe (Sturm and Holmgren, 2018). The magnaprobe consists of a 1.3 m long ~1 cm diameter rod with a moveable basket that uses a GPS and a magneto restrictive material inside the rod to record snow depth and location in seconds (Sturm and Holmgren, 2018). GPS horizontal location accuracy is ± 2.5 m in open areas but may decrease to 10–15 m in dense forest (Douglas and Zhang, 2021; Sturm and Holmgren, 2018). Snow depth measurements were taken at four sample locations within the CPCRW (Fig. 1); measurements were used as validation points
125 to determine the accuracy of the lidar-derived snow depth map.

Two additional snow depth measurements were obtained from snow course sites operated by the USDA Natural Resources Conservation Service (NRCS) within CPCRW (Fig. 1). Snow depth records date back to December 1969 at both sites with the 30 year (1991–2020) median snow depths available for the start of each month. At the start of March, the 30-year median snow depth for the Caribou Creek snow course was 58 cm, and for the Caribou Snow Pillow snow course was 56 cm (USDA
130 Natural Resources Conservation Service, 2023). Snow depths recorded on 1 March 2022, from the Caribou Creek and Caribou Snow Pillow snow course sites were compared to the SnowEx Alaska ground-based and lidar-derived snow depth values collected on 11 March 2022.

2.2.2 Airborne Lidar

Airborne lidar, an active remote sensing system, records the time required for emitted light to travel to the ground and back to
135 an airplane-mounted sensor. The sensor includes a GPS that identifies the X,Y,Z location of the light energy, and an internal measurement unit that provides the orientation of the plane in the sky. The resultant data can be used to create a high-resolution digital terrain model (DTM) that approximates a bare earth surface. Differencing a snow-free from a snow-on surface elevation data set allows for a straightforward mapping of snow depth. In addition to providing spatial data on snow distribution, airborne lidar can produce spatial data of canopy heights by subtracting a bare-earth digital terrain model from a digital surface model
140 (DSM). A DSM models the canopy and the top of the vegetation by accounting for all the first, or only, lidar pulses returned to the sensor.

Two airborne lidar surveys were flown over CPCRW (Larsen, 2024). The first was flown prior to the onset of snow melt on 11 March 2022. The second was flown on 29 May 2022, during snow-free conditions. The lidar flight area of coverage is represented by the red box in Fig. 1 and constitutes the study site. All references to CPCRW and all statistical analysis performed in this study are in reference to the larger area within the lidar box, not the boundary of the watershed (Fig. 1). The 11 March 2022, lidar survey occurred concurrent with ground-based snow depth measurements taken on the same day. Differencing the May snow-free DSM from the May snow-free DTM produced a lidar-derived canopy height map.

The lidar and stereophotogrammetry instruments are combined on rigid mount and deployed simultaneously in a Cessna T206 aircraft. The lidar scanner uses a 1064 nm wavelength laser and has adjustable pulse repetition frequency up to 2000 kHz. The scanner has a rotating mirror that sweeps the beam across 75 degrees (+/- 37.5 degrees off nadir), resulting in shot lines perpendicular to the flight path (MacGregor et al., 2021). Flight lines are planned with > 50% sidelap to target 20 points per square meter for each survey coverage. The vertical and horizontal accuracy of the lidar snow depth and canopy height maps is ± 5.0 cm.

3 Methods

3.1 Lidar Data Review

The lidar data products were reviewed for quality control and visually inspected for abnormalities. Lidar snow depth and canopy height pixel values that represented unlikely snow depths or canopy heights for the CPCRW, or that displayed abnormal distribution patterns, were removed from the analysis. Negative pixel values, which are usually the result of error points in one of the lidar data sets, were assigned a "no data" code during quality control.

The lidar snow depth map contained pixel values ranging from -300 cm to 499 cm, an implausible range in snow depths for CPCRW. We analyzed ground-based SnowEx snow depths, the NRCS snow course measurements, and a histogram of the lidar snow depths to determine a plausible snow depth range for CPCRW. A color scale map of the lidar snow depths was generated to observe if identifiable patterns existed that indicate where unlikely snow depth values appeared. The lidar snow depth map was then corrected to include only pixels occurring within the plausible snow depth range, and all remaining pixels were classified as "no data."

The lidar canopy height map contained pixel values ranging from -3 m to 40 m. All positive canopy height values were included in the analysis and classified according to the vegetation found within CPCRW. Canopy height classes were determined after referencing the vegetation classification used in the U.S. Geological Survey National Land Cover Database (NLCD) 2016 Land Cover - Alaska (ver. 2.0, July 2020) (Dewitz, 2019) and the Fuel Model Guide to Alaska Vegetation (Alaska Fuel Model Guide Task Group, 2018).

3.2 Lidar Data Reduction

The lidar snow depth and canopy height rasters contain approximately 86 million positive pixels each. After the snow depth and canopy height maps were reviewed and corrected, a size reduction of both rasters was necessary for practical processing times during the statistical analysis.

175 The first data reduction technique used for the statistical analysis was to determine the distance at which snow depths were no longer spatially autocorrelated. To determine spatial autocorrelation, 15 smaller sections of the lidar snow depth map were portioned, and a semivariogram was developed for each section. The range value of each semivariogram was estimated using the Ordinary Kriging (OK) interpolation method. Ordinary Kriging is a frequently used interpolation method for estimating snow depth because it is easy to implement, considers the variables of variation and distance between points, and assumes a

180 constant mean (Ashtiani, 2024; Carroll and Cressie, 1996; Erxleben et al., 2002; Huang et al., 2015; Lloyd and Atkinson, 2001; Ohmer et al., 2017; Tabari et al., 2010). The semivariogram ranges were then averaged over the fifteen sections, and the lidar snow depth map was resampled, applying the semivariogram range to effectively eliminate spatial autocorrelation from contiguous pixels. The resulting snow depth map displays the independent snow depths required for the statistical analysis. The lidar canopy height map was resampled to the same resolution as the new snow depth map with corresponding pixel sizes.

185 To further reduce the lidar snow depth map to a size that allowed for practical processing times, three spatial subsets were created. Each spatial subset exhibited land cover and canopy height percentages comparable to those of the entire study site. The resampled lidar snow depth and canopy height maps were then clipped with each spatial subset. The clipping allowed the lidar snow depth map to be reduced from 86 million pixels to approximately 2 million pixels for each spatial subset. The lidar-derived snow depths from each spatial subset were used in the statistical analyses and the lidar canopy height data was utilized

190 for classification purposes.

To compare the lidar snow depths with collocated ground-based measurements, ground-based snow depth coordinates were obtained from the magnaprobe's GPS. Using the ground-based coordinates, a corresponding lidar snow depth was obtained for each ground-based measurement. Lidar data review, reduction, analysis, and comparison with ground-based measurements was performed using ArcGIS Pro software.

195 ### 3.3 Statistical Analysis

The statistical analysis was performed with the reduced lidar snow depth data. The Kruskal–Wallis statistical test was conducted to determine if a statistically significant difference in average snow depth existed between canopy height classes. The standard One-Way Analysis of Variance (ANOVA) test was not used because normality of the residuals was not satisfied, as determined by the shape of the normal Q-Q plots for each subset. The Kruskal–Wallis test is the non-parametric equivalent

200 of the ANOVA, does not assume normality in the data, and it is much less sensitive to outliers than the ANOVA (Kruskal and Wallis, 1952).

Assumptions for the Kruskal–Wallis test are: continuous response variable, independence, and that distributions have similar shapes (Kruskal and Wallis, 1952). The assumption of independence was met by thinning the data according to the semivariogram range. The assumption of similarly shaped distributions was verified through basic histogram examination. The null hypothesis states that all the median snow depths among canopy height classes are equal.

The Kruskal–Wallis test uses the ranks of the data to calculate the test statistic, H, given by Eq. (1):

$$H = \left[\frac{12}{n(n+1)} \sum_{j=1}^{c} \frac{T_j^2}{n_j} \right] - 3(n+1) \,, \tag{1}$$

where n is the total sample size (number of snow depths), c is the number of groups (canopy height classes) we are comparing, T_j is the sum of ranks for group j, and n_j is the sample size of group j (number of snow depths within the canopy height class). H is then compared to a critical cutoff point determined by the chi-square distribution with (c-1) degrees of freedom. The chi-square is the sum of the squared deviations and is applied for accurate approximation of the distribution of H under the null hypothesis. If significant deviations are present, then the chi-square is large, and the p-value is small enough to be considered evidence of significant deviations from chance (Diez and Barr, 2012). If the H statistic is significant (H is larger than the cutoff) then the null hypothesis is rejected. If the H statistic is not significant (H is smaller than the cutoff) then the null hypothesis is retained. The Kruskal–Wallis test was applied to obtain the chi-square and p-values. A p-value less than 0.05 indicates a statistically significant difference between the median snow depths for all groups.

To further characterize significance, the empirical Wilcoxon Rank Sum test was next applied to determine which canopy height pairs have significantly different median snow depths from each other and to compute the pairwise difference in median snow depths between each pair. The three canopy height pairs used in the Wilcoxon Rank Sum test are: forest and SSS, forest and treeless, and SSS and treeless. The result will be used to determine what effect canopy height has on snow depth variability in the study site. The Wilcoxon Rank Sum test is a non-parametric alternative to the two sample t-test. It has two assumptions: independence and equal variance (Mann and Whitney, 1947). Independence was met by thinning the data while equal variance was verified using histograms. The Wilcoxon test is based upon ranking the $n_1 + n_2$ observations of the combined sample. Each observation has a rank: the smallest has rank 1, the 2nd smallest rank 2, and so on (Mann and Whitney, 1947). The null hypothesis of the Wilcoxon Rank Sum test states that the median snow depths of the two samples are the same.

The test statistic for the Wilcoxon Rank Sum test is denoted by U and defined as the smaller of U_1 and U_2 below in Eq. (2) and Eq. (3):

$$U_1 = n_1 n_2 + \frac{n_1(n_1+1)}{2} - R_1 \tag{2}$$

$$U_2 = n_1 n_2 + \frac{n_2(n_2+1)}{2} - R_2 \tag{3}$$

where R_1 = sum of the ranks for group 1 and R_2 = sum of the ranks for group 2 (Mann and Whitney, 1947). The test was run to calculate the p-value, indicating a statistically significant difference in median snow depths between the two sampled classes. The differences of medians were computed for each vegetation class pair. The Kruskal–Wallis and Wilcoxon Rank Sum tests

was run using the R-4.1.2 statistical programming environment (R Core Team, 2022) to obtain corresponding chi-square and p-values for each spatial subset.

4 Results

4.1 Canopy Height Classes

Three canopy height classes were selected to study the effect of vegetation on snow depth variability: 1) forest, 2) shrub and short stature trees (SSS), and 3) treeless. Vegetation pixels with a lidar canopy height greater than 5.0 m were classified as "forest"; forest pixels constituted 25.9 % of the study area (Fig. 2). Vegetation pixels with a lidar canopy height ranging between 0.2 m and 5.0 m were classified as "SSS," and pixels with a lidar canopy height of less than 0.2 m were classified as "treeless." SSS pixels constituted 27.1 %, and treeless pixels constituted 47.0 % of the study site (Fig. 2). The percentage of canopy height pixels for each of the watershed subbasins can be found in Table 1. Subbasins P3 and P5, within the Poker Creek watershed, contain the highest percentage of forest pixels. The southernmost subbasin for each watershed, P6 and C3, contain the highest SSS pixels, and subbasins P6 and C2 contain the highest treeless pixels. The three canopy height classes were used to classify ground-based and lidar-derived snow depths in the statistical analysis. Photographs of the study site showing vegetative examples of each canopy height classification without snow cover can be found in Fig. 3.

Table 1: Canopy height percentages for each of the watershed subbasins located within the CPCRW.

Subbasin	Forest Pixels	SSS Pixels	Treeless Pixels
P1	31.5 %	31.9 %	36.6 %
P2	34.4 %	27.2 %	38.4 %
P3	47.2 %	23.5 %	29.3 %
P4	26.8 %	25.6 %	47.6 %
P5	52.0 %	20.5 %	27.5 %
P6	14.2 %	35.7 %	50.1 %
C1	28.2 %	31.7 %	40.1 %
C2	32.4 %	13.8 %	53.8 %
C3	23.2 %	35.5 %	41.3 %
C4	37.5 %	21.8 %	40.7 %
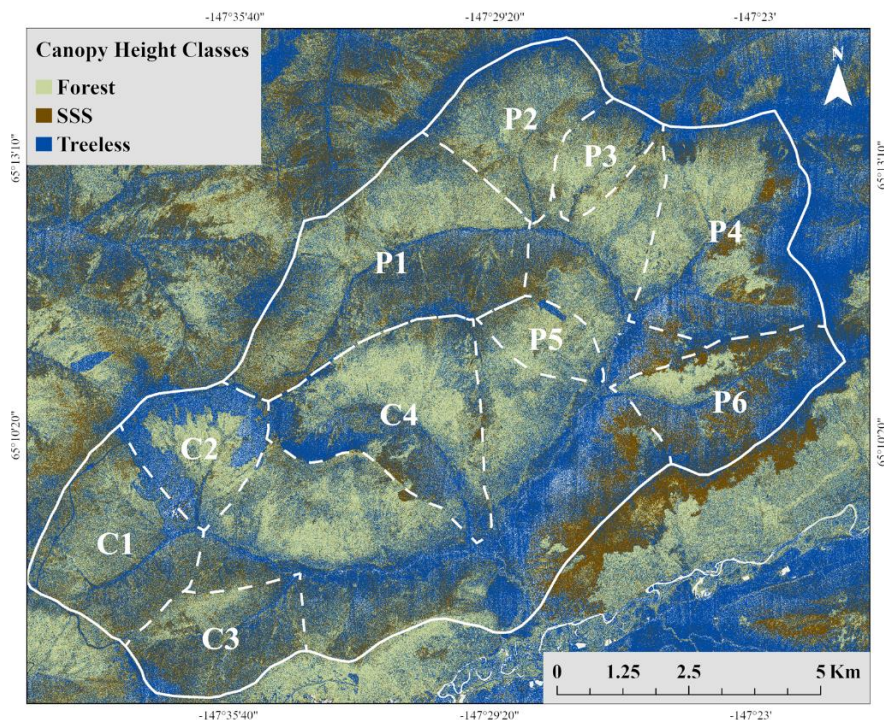
Figure 2: Canopy height map with color scale applied to show canopy height class distribution and subbasins (dashed white lines) within CPCRW (solid white line).
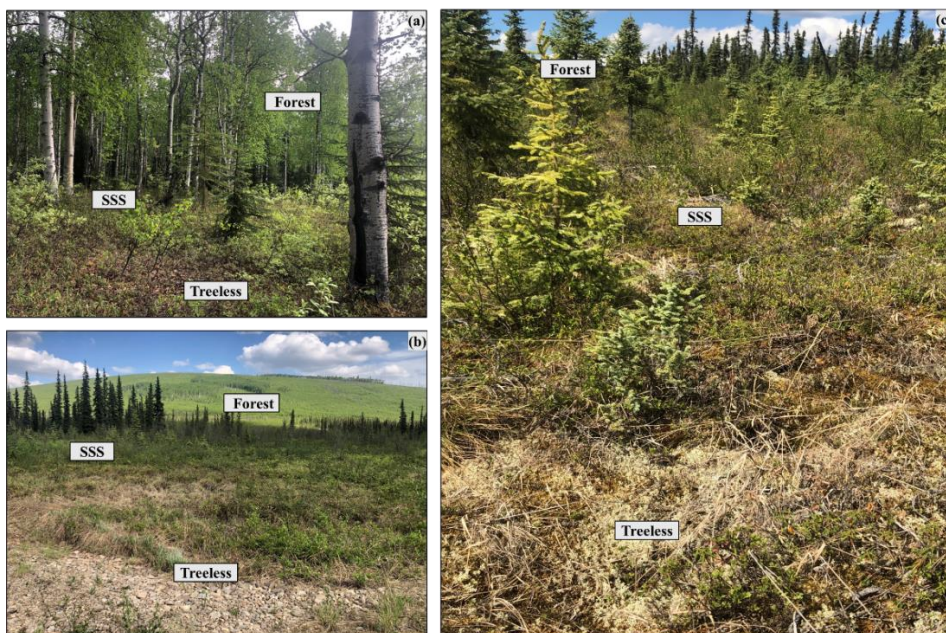
Figure 3: Photographs of the vegetative land cover taken in CPCRW on 2 June 2022, showing forest and understory examples of each canopy height class.

4.2 Comparison of Ground-Based and Lidar-Derived Snow Depths

Ground-based snow depth measurements covered approximately 1.0 % of the total area of the watershed. The mean for all ground-based snow depths in the study site ($\overline{HS}$=88 cm) was similar to the mean snow depth calculated for ground-based measurements classified by canopy height (forest ($\overline{HS}$=85 cm), SSS ($\overline{HS}$=87 cm) and treeless ($\overline{HS}$=88 cm)) (Table 2). The
260   range for all ground-based snow depths was 23–121 cm (Table 2).

During March 2022 the snow depth at the USDA Caribou Snow Pillow snow course was 94 cm. This represents a 61 % increase from the 30-year median snow depth of 58 cm. At the USDA Caribou Creek snow course, the March 2022 snow depth was 89 cm, a 59 % increase from its 30-year median of 56 cm (USDA Natural Resources Conservation Service, 2023). These statistics demonstrate 2022 as an above-normal snowpack year.

265

Table 2: The mean manual snow depth ($\overline{HS}$), range, standard deviation (SD) and number of ground-based measurements (n) recorded for the CPCRW and each canopy height class.

Class	n	$\overline{HS}$ (cm)	Min HS (cm)	Max HS (cm)	SD (cm)
All CPCRW	2,114	88	23	121	9.4
Forest	177	85	42	99	8.7
SSS	236	87	29	100	10.6
Treeless	1464	88	23	121	9.3

270   The lidar data review resulted in a plausible snow depth range of 0–180 cm, which represents 99.98 % of the snow-covered area sampled by lidar. The remaining 0.02 % are pixels that were located surrounding gaps (no data pixels) in the lidar, adjacent to structures, along trails, or scattered in patterns that do not reflect natural snowpack conditions. These pixels were omitted from the analysis.

Ground-based and lidar-derived snow depths were compared to quantify lidar accuracy and analyze snow depth variability
275   within the study site. The average lidar-derived snow depth and standard deviation at in situ (ground-based) locations, the study site, and each canopy height class can be found in Table 3. For the study site, the mean lidar snow depth was calculated to be 98 cm (Table 3). The mean lidar snow depth at in situ locations was 90 cm. As suggested by this research, the sample variance of snow depths from airborne lidar minimally exceeds the sample variance from ground-based snow depths at the study site. The mean lidar-derived snow depths at collocated in situ locations was 2 cm more than the magnaprobe
280   measurements from March 2022, and the mean lidar snow depth for the entire study site was 10 cm more than the magnaprobe measurements. Calculated standard deviations indicate that ground-based snow depth measurements vary by 9 cm, whereas lidar-derived snow depths for the study site vary by 15 cm. At the subbasin level, the mean lidar snow depths for all subbasins varied by 11 cm, with standard deviations ranging from 12–17 cm (Fig. 4). When comparing mean snow depths with the two

snow course snow depths (89 cm and 94 cm), ground-based mean snow depths were all lower, while mean lidar snow depths
285   were all between, or above, the snow course snow depths. The mean lidar snow depths for canopy height classes increased by
5 cm for forest, 15 cm for SSS, and 14 cm for treeless when compared to the corresponding mean snow depth at in situ locations
based on canopy height. A whisker and box plot representing the mean lidar snow depth and standard deviation for the
subbasins is found in Fig. 4.

290   **Table 3: The mean lidar-derived snow depth ($\overline{HS}$), standard deviation (SD), and number of lidar pixels (n) for the study site and canopy height classes.**

Class	n	Lidar $\overline{HS}$ (cm)	Lidar SD (cm)
At In situ Locations	2,114	90	8.8
All CPCRW	86 million	98	15.3
Forest	22 million	90	13.3
SSS	23 million	102	14.6
Treeless	40 million	102	14.9

To quantify lidar accuracy, lidar-derived snow depths and concurrent ground-based snow depths were compared statistically.
295   A scatterplot for all ground-based and lidar-derived snow depths, and a corresponding 1:1 line, is displayed in Fig. 5. Error
statistics from the lidar validation analysis produced a bias of 2.0 cm, an RMSE of 12.0 cm, and an R^2 value of 0.012 (Fig. 5).
Error statistics and scatterplots for ground-based and lidar-derived snow depths based on canopy height resulted in a bias of 2
cm, and an RMSE of 12 cm for SSS and treeless, and a bias of 0 cm and an RMSE of 12 cm for forest (Fig. 5). All three canopy
height classes had low R^2 values (Fig. 5).

300
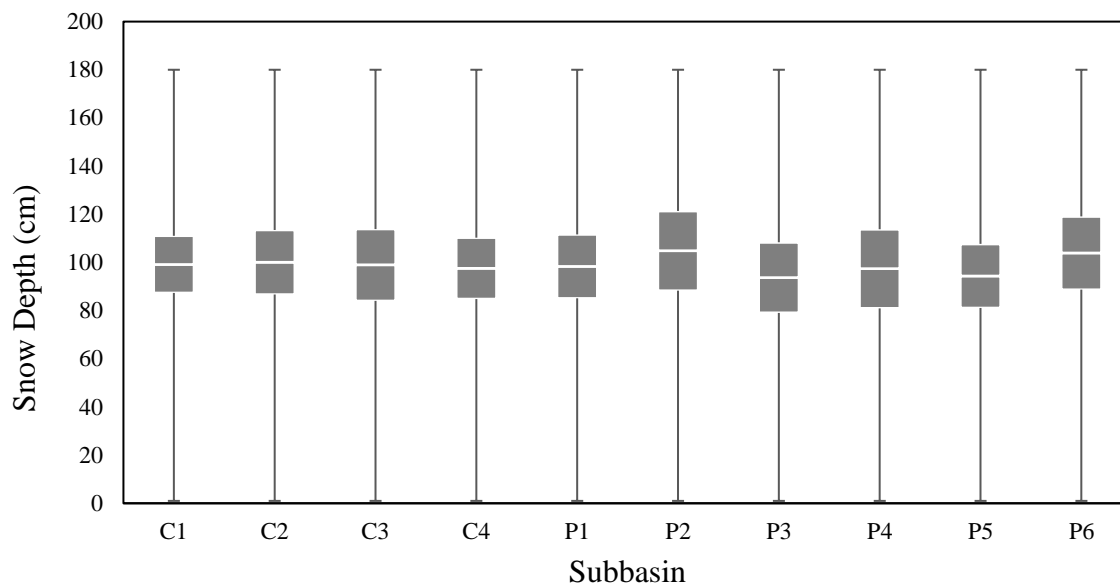
Figure 4: Whisker and box plot representing lidar snow depths within each subbasin in the CPCRW. The white bar represents the mean lidar snow depth, the grey boxes represent the ± standard deviation, and the whiskers represent the minimum and maximum lidar snow depth within each subbasin.

305
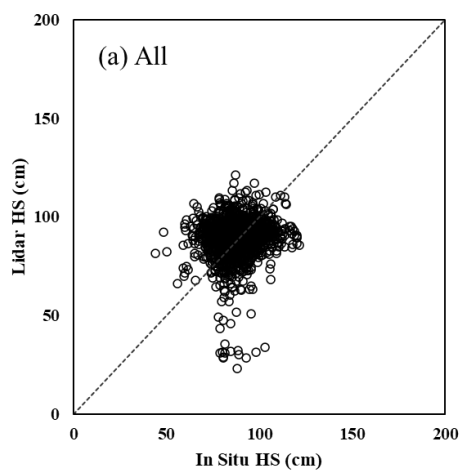
Bias: 2 cm; RMSE: 12 cm; R²: 0.012   Bias: 0 cm; RMSE: 12 cm; R²: 0.012

Bias: 2 cm; RMSE: 12 cm; R²: 0.042   Bias: 2 cm; RMSE: 12 cm; R²: 0.003
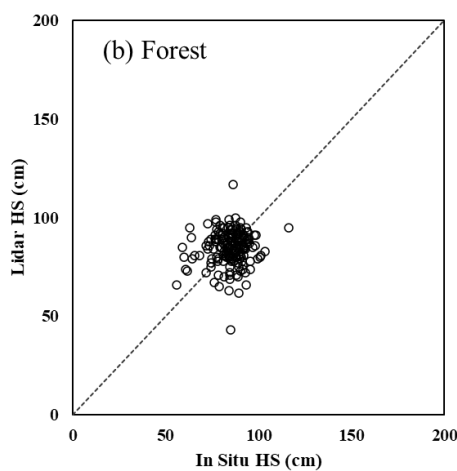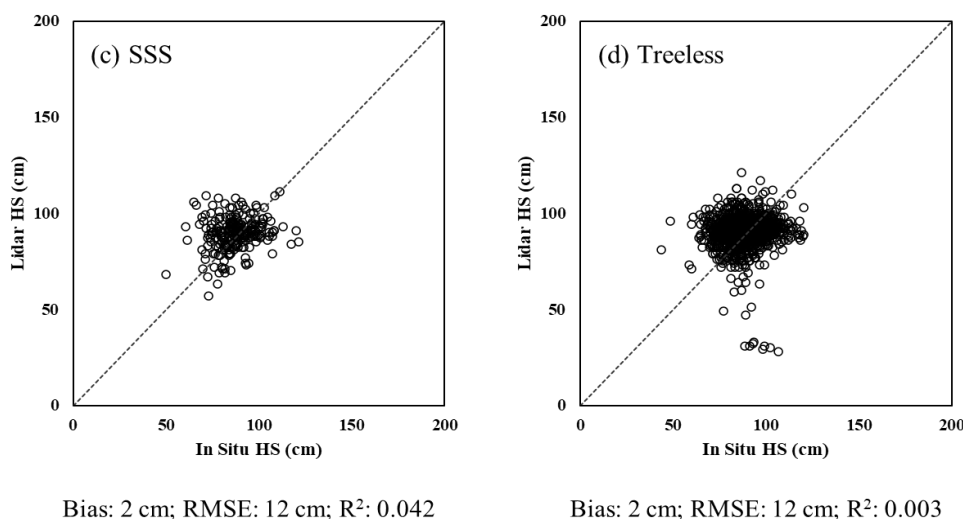
Figure 5: Scatterplots comparing ground-based snow depths with collocated lidar snow depths with a corresponding 1:1 line for all
310 **ground-based measurements within CPCRW (a), and for ground-based measurements classified as forest (b), SSS (c), and treeless (d) canopy height classes. Error statistics for each classification are displayed.**

4.3 Statistical Analysis of Lidar-Derived Snow Depths based on Canopy Height

To statistically compare lidar-derived snow depths between canopy height classes, it was necessary to create a snow depth
315 map with independent observations that had eliminated spatial autocorrelation. The semivariogram analysis showed the average semivariogram range for the lidar-derived snow depth map to be 1.0 meter. The lidar snow depth map was resampled to a 1.5 m spatial resolution to eliminate spatial autocorrelation. The lidar canopy height map was resampled to a 1.5 m spatial resolution to correspond to the lidar snow depth map pixel size.

The lidar-derived snow depths and canopy heights from the three spatial subsets were used as variables to run the statistical
320 Kruskal–Wallis test. Results of the Kruskal–Wallis test (Table 4) show that the p-values comparing lidar-derived snow depths with canopy height are below the required value for significance (p-value < 0.05). A small p-value and a large chi-square statistic allowed for a rejection of the null hypothesis, which states that the median lidar-derived snow depths between the canopy height classes are equal. A rejection of the null hypothesis supports the finding that there is a statistically significant difference in snow depths between canopy height classes for all three spatial subsets.

325

Table 4: Results of the Kruskal–Wallis test comparing median lidar snow depths based on canopy height class for each subset.

	Chi-squared	P-value
Subset 1	**329,932**	**< 2.2 e - 16**
Subset 2	**263,750**	**< 2.2 e - 16**

Subset 3	51,595	< 2.2 e - 16

After a statistically significant difference in lidar-derived snow depths for the three spatial subsets was determined, the
330 Wilcoxon Rank Sum test was used to calculate the p-value of the median snow depth between specific canopy height pairs. The results of the Wilcoxon Rank Sum test show a statistically significant difference (p-value < 0.05) in the snow depth medians between each canopy height pair (SSS and forest, treeless and forest, and treeless and SSS) for all three subsets (Table 5).

335 **Table 5: Results of Wilcoxon Rank Sum test comparing the median lidar snow depth between canopy height pairs for each spatial subset.**

Subset 1 and Subset 3		
	Forest	**SSS**
SSS	< 2e-16	—
Treeless	< 2e-16	< 2e-16

Subset 2		
	Forest	**SSS**
SSS	< 2e-16	—
Treeless	< 2e-16	<6.2e-5

4.4 Influence of Canopy Height on Snow Depth Estimation

To analyze the influence of canopy height on snow depth distribution within the study site, the snow depth difference between
340 specific canopy height pairs was calculated. This result was accomplished by observing the pairwise difference in median snow depths calculated by the Wilcoxon Rank Sum test. The pairwise difference value was used to estimate the lidar snow depth variability between each canopy height pair. The difference in mean lidar-derived snow depths between each canopy height pair for the three spatial subsets is shown in Table 6. Two canopy height class pairs, SSS and forest, and treeless and forest, had mean snow depth differences that were greater than the ±5 cm lidar vertical accuracy range for all three spatial
345 subsets. When comparing the mean snow depth differences between these two class pairs, SSS averaged 9–14 cm more snow than forest (Table 6), and treeless averaged 12–14 cm more snow than forest (Table 6) for all three spatial subsets. This difference in snow depths is equivalent to an SWE range of 0.02–0.03 m. Canopy height SSS averaged slightly less snow than treeless, but the mean snow depth differences for the three spatial subsets fell within the ±5 cm lidar vertical accuracy range.

350 **Table 6: Difference in mean lidar-derived snow depth between canopy height class pairs. The mean snow depth of the second class listed is subtracted from the mean snow depth of the first class listed.**

Canopy Height Pair	Subset 1 difference (cm)	Subset 2 difference (cm)	Subset 3 difference (cm)
SSS - Forest	9.0	14.0	9.0

Treeless - Forest	12.0	14.0	13.0
Treeless - SSS	3.0	0.1	4.0

5 Discussion

5.1 Sources of error and uncertainty in lidar derived snow depths

355   Ground-based snow depth measurements provide an independent data set for the assessment of errors and uncertainties in data collected remotely. Ten studies that used ground-based measurements to validate airborne lidar (Table 7) in forested areas found RMSE's ranging from 3 cm to 37 cm. Koutantou et al., (2022) found that their boreal forest site had the highest RMSE (19–22 cm) compared to their deciduous forest and field sites. This study's calculated RMSE for comparing lidar-derived snow depths with ground-based measurements (RMSE=12.5 cm) falls within a range that is generally acceptable for most research

360   (Harpold et al., 2014). A prominent non-processing source of error in airborne lidar data is vegetation-induced errors (Deems et al., 2013). Vegetation-induced errors can be minimized by increasing the pulse rates and decreasing the scan angles (Campbell et al., 2018; Deems et al., 2013). The lidar scanner used in this study had a pulse repetition frequency up to 2000 kHz and an angle scan of 75 degrees. The higher pulse rate increases the probability of sufficient laser shots penetrating the canopy, reaching the ground, and returning to the sensor. Deems et al. (2013) found that the ground return point density

365   decreases inversely with canopy and subcanopy density and is influenced by canopy and understory structure. We suggest that error between our lidar-derived and ground-based snow depth measurements are primarily due to vegetation, specifically the dense understory, rather than errors associated with lidar processing techniques.

   The dense understory canopy height classes of SSS and treeless, that make up approximately 74 % of CPCRW (Fig. 3), interfere with lidar laser pulses to penetrate to, and accurately map the ground surface. Reutebuch et al. (2003) found that when

370   using airborne lidar to measure ground elevations in a forested area, the accuracy of the ground points was reduced by approximately 10 cm because the dense canopy and understory vegetation reduced the strength of the return signal back to the sensor, making it harder to precisely pinpoint the ground surface. Prior studies noted similar lidar errors occurring in vegetative landscapes where shrubs were prominent (Contreras et al. 2017; Gould et al., 2013; Spaete et al., 2011). We believe that the view of the lidar sensors used in this study were occluded by the dense understory vegetation, weakening the lidar signal and

375   preventing it from accurately mapping the ground surface. During snow-on acquisition dense ground vegetation could further introduce error into the snow-on DEM by compacting beneath the snowpack, or elevating snow on top of dense vegetation. Errors in both snow-free and snow-on DEMs caused by the dense understory can lead to a less accurate snow depth map, which in turn affects the correlation between ground-based and lidar-derived snow depth measurements.

   The coefficient of determination between ground-based and lidar-derived snow depths (R^2=0.012) is considerably lower for

380   this study, compared to the studies listed in Table 7. Possible explanations for a low R^2 value are that ground-based snow depth measurements were clustered together and represented only a small portion of CPCRW (approximately 1 % of the study area).

The magnaprobe GPS units have a horizontal positioning error of 2.5 m in open areas and 10–15 m in dense forest which could impact the correlation of ground-based snow depths with collocated lidar-derived snow depths. Lastly, snow depth variability is dependent on the spatial scale. During the March 2022 Snow Ex field campaign, evidence of snow depth variability over a

385   single meter of distance was repeatedly seen in the field while taking ground-based measurements. Tussocks, understory brush, downfall, and the snowpack itself all impacted snow depths within a meter. Ground-based snow depth variability observed in the field, on a small spatial scale, supports the calculated semivariogram range of 1.0 m for spatial autocorrelation. However, when comparing snow depth variability over a larger spatial scale, the entire study area, all ground-based, lidar, and canopy height mean snow depths fell within one standard deviation of each other and had low standard deviation ranges (9–15 cm).

390   Results from an analysis performed using ground-based and airborne lidar data from the March 2023 SnowEx Alaska campaign for this study site found similar statistical results (R^2=0.048 and SD is 11–14 cm). Demonstrating a consistent low variation in snow depths over the two snowpack years at this study site, despite mean snow depths being statistically significantly different from each other.

395   **Table 7: Studies that compared lidar-derived snow depths with manual snow depth measurements are listed in the table. Information on location, landcover type, manual and lidar snow depth means, and error statistics are provided for each study.**

Study	Location	Landcover	HS Mean (cm)	RMSE (cm)	R^2
Broxton et al., 2015	Colorado and New Mexico	Forest/Canopy cover	CO: mean 63 (manual) mean 74.8 (modelled) NM: mean 88 (manual) mean 93 (modelled)		0.01–0.33
Broxton et al., 2019	Central Arizona	Forest	Mean 44 – 49 (manual)	9.1–18.7	0.85–0.91
Currier et al., 2019	Grand Mesa, CO	Forest	Manual mean 6 cm greater than lidar mean	8	
Dharmadasa et al., 2022	Southern Quebec	Forest/Boreal Forest	Mean 32–140 (manual)	7.9–22	
Harpold et al., 2014	California, Colorado, New Mexico	Forest/Alpine	Mean 0–274 (manual) Mean 7–222 (lidar)	7–31	0.97
Hopkinson et at., 2004	Southern Ontario, Canada	Forest	Mean 42 (manual)		0.52
Hopkinson et al., 2012	Southern Alberta, Canada	Forest/Canopy cover	Mean 54 (manual) Mean 60 (lidar)		0.74

Jacobs et al., 2021	New Hampshire	Mixed hardwood forest	Mean 15.2 (manual) Mean 7.8 (lidar)	10.5	
Koutantou et al., 2022	Swiss Alps	Forest		5–21	0.6–0.8
Tinkham et al., 2014	Southwest Idaho	Forest/Shrub	Mean 114 (manual) Lidar mean 5–7 cm greater than manual	14–38	
This study	Fairbanks, Alaska	Boreal Forest	Mean 88 (manual) Mean 98 (lidar)	12.5	0.012

5.2 Implications for Water and Resource Management

400 Water and resource managers use snow data, including snow depth and SWE, to assess the availability of water resources in regions dependent on snowmelt (Dickerson-Lange et al., 2021; Siirila-Woodburn et al., 2021). Our study site had a mean lidar snow depth of 98 cm, which is equivalent to approximately 0.21 m of SWE. When comparing median snow depths our analysis showed a statistically significant difference in median snow depths between all canopy height classes, with differences in snow depths, based on canopy height, equivalent to a SWE range of 0.02–0.03 m. This information can be utilized by water and

405 resource managers to make informed decisions about water supply, flood control, evaluating the impact of climate change on precipitation and snow accumulation/melt patterns, land use decisions, and wildlife and conservation efforts (Dickerson-Lange et al., 2021; Hopkinson et al., 2004; Mazzotti et al., 2019; Reinking et al., 2022; Webb et al., 2020).

Snow data obtained through various platforms, including ground-based, aircraft, satellite, or estimated through modelling tools, can be incorporated together to produce more accurate and sophisticated spatiotemporal snow distributions estimations than

410 are possible with any single measurement technique performed alone (Boelman et al., 2019; Stuefer et al., 2013). This study used ground-based measurements to validate an airborne lidar snow depth map in a boreal forest ecotype. As evidenced in Table 7, only one additional study that compared ground-based measurements to airborne lidar occurred within a boreal forest site. The comparison of ground-based measurements to airborne lidar by Dharmadasa et al., (2022), produced an RMSE of 19–22 cm at their boreal forest site. This study produced an RMSE of 12.5 cm when validating airborne lidar with ground-

415 based snow depth measurements. Validated lidar snow depth maps have advanced our ability to characterize the spatiotemporal variability in snow depths at a watershed scale, and when coupled with an airborne lidar canopy height map, can be applied to snow and hydrological modeling applications to improve hydrological forecasts and SWE estimates at even larger regional or global scales (Deems et al., 2013; Hopkinson et al., 2004, 2012; Jacobs et al., 2021; Nolan et al., 2015; Painter et al., 2016; Trujillo et al., 2007). To further improve validated lidar snow depth maps, future snow research occurring in boreal forests

420 should include snowpack profile measurements that could be used to identify and quantify vegetation-induced errors in ground-

based measurement techniques and airborne lidar data products associated with the complicated and dense boreal forest understory.

Accurately accounting for vegetation effects on snow storage and distribution is important as forests are changing due to warming climate conditions, forest disturbances, wildfires, insect infestation, and permafrost degradation (Panda et al., 2010; 425 Smith et al., 2021). These changes are occurring in boreal forests, but research is limited as to how Alaska boreal forest vegetation impacts snow distribution. A literature review found one study occurring in an Alaska boreal forest, by Douglas et al., (2021), that looked at vegetation impacts on snow storage using lidar and machine learning. They found that in their Alaska boreal forest sites mixed forest ecotypes had the shallowest snowpack, while tussock tundra (equivalent to our treeless) and moss spruce forest (equivalent to our SSS) were associated with the deepest snowpack. The results of our vegetation analysis 430 show that canopy height has a statistically significant effect on the spatiotemporal variability of snow depths at our study site. The canopy height pairs of SSS and forest and treeless and forest, had snow depth differences that fell outside the lidar error range for all three spatial subsets, exhibited greater variability based on standard deviations, and differed in SWE by 0.01 m. The canopy height pair of treeless and SSS yielded results that fell within the lidar error range for all three spatial subsets, making it difficult to clearly attribute snow depth variability between the two classes to vegetation or lidar accuracy. This 435 result implies that there is little variability in snow depths between treeless and SSS canopy height classifications. We suggest that two canopy height classes of less than 5 m and greater than 5 m would be sufficient to accurately quantify the spatial variability of snow depths and SWE in boreal forests.

6 Conclusion

Despite considerable literature on airborne lidar snow depth retrievals in forested environments, little research has been 440 published on its ability to measure snow depth in boreal forests. We demonstrate the utility of a high-resolution airborne lidar snow depth map to characterize the spatial variability of snow depths within a boreal forest study site where snow remote sensing research is limited. The validation efforts showed lidar-derived snow depths had an RMSE of 12.0 cm, and a bias of 2.0 cm, when compared to data from 2,114 ground-based field measurements. While these results show a statistically significant relationship between lidar-derived snow depths and manual field measurements, errors and uncertainties caused by 445 dense understory vegetation need to be considered with detailed snowpack profile measurements. We further demonstrate that an airborne lidar canopy height map can be used to analyze the impact of vegetation on snow depth variability in a complex boreal forest ecosystem, and that two canopy height classes may be sufficient to characterize the snow depth spatial variability therein.

Lastly, we show that snow depth variability within the study site, between subbasins, and between each canopy height class, 450 is low. This is evidenced by all mean snow depths (ground-based, lidar, canopy height class, subbasins, and overall) falling within one standard deviation of each other. This study demonstrates that airborne lidar-derived data products can effectively

estimate and quantify the variability of snow depths in an Alaska boreal forest but should be validated and assessed for vegetative errors using ground-based measurements.

Data Availability

The airborne lidar data (Larsen et al., 2024) and the magnaprobe data (May et al., 2024) used for validation were obtained from the National Snow and Ice Data Center (NSIDC). The SNOTEL data for the two snow courses located within the study site can be accesses at https://www.nrcs.usda.gov/alaska/snow-survey.

Author Contribution

Svetlana Stuefer and Lora May conceptualized this project, and Svetlana Stuefer acquired the funding and supervised the project. Lora May performed the formal analyses and prepared the manuscript. Scott Goddard assisted in statistical analysis and wrote the statistical processing codes. Christopher Larsen collected, processed, and shared the airborne lidar data products. Svetlana Stuefer, Scott Goddard, and Christopher Larsen reviewed and edited the manuscript.

Competing Interests

Svetlana Stuefer is a guest editor for this special issue.

Acknowledgements

This project was funded by NASA SnowEx grants 80NSSC21K1913, 80NSSC23K1419, and 80NSSC21M032. We thank the SnowEx communities for the extensive field work in collecting snow depth measurements and their insight into how remote sensing techniques can be applied to snow science. We give additional thanks to Sandra Boatwright for her expertise in editing this manuscript.

References

Alaska Fuel Model Guide Task Group: Fuel Model Guide to Alaska Vegetation, Unpubl. Report, Alaska Wildland Fire Coordinating Group, Fire Modeling and Analysis Committee, Fairbanks, AK, USA, https://fire.ak.blm.gov/content/admin/awfcg/C.%20Documents/Revised%20Alaska%20Fuel%20Model%20Guide%202018-05-22.pdf, 2018.

Ashtiani, Z. and Deutsch, C. V.: https://geostatisticslessons.com/lessons/krigingconstraints, Kriging with Constraints, Geostatistics Lessons, Geostatisticslessons.Com. 2024. Last access: 27 October 2024.

Askne, J. I. H., Soja, M. J., and Ulander, L. M. H.: Biomass estimation in a boreal forest from TanDEM-X data, lidar DTM,
480   and the interferometric water cloud model, Remote Sens. Environ., 196, 265–278, https://doi.org/10.1016/j.rse.2017.05.010, 2017.

Barnett, T., Malone, R., Pennell, W., Stammer, D., Semtner, B., and Washington, W.: The effects of climate change on water resources in the west: Introduction and overview, Climatic Change, 62, 1–11,
485   https://doi.org/10.1023/B:CLIM.0000013695.21726.b8, 2004.

Barnett, T. P., Adam, J. C., and Lettenmaier, D. P.: Potential impacts of a warming climate on water availability in snow-dominated regions, Nature, 438, 303–309, https://doi.org/10.1038/nature04141, 2005.

490   Boelman, N. T., Liston, G. E., Gurarie, E., Meddens, A. J. H., Mahoney, P. J., Kirchner, P. B., Bohrer, G., Brinkman, T. J., Cosgrove, C. L., Eitel, J. U. H., Hebblewhite, M., Kimball, J. S., Lapoint, S., Nolin, A. W., Pedersen, S. H., Prugh, L. R., Reinking, A. K., and Vierling, L. A.: Integrating snow science and wildlife ecology in Arctic-boreal North America, Environ. Res. Lett., 14(1), 010401, https://doi.org/10.1088/1748-9326/aaeec1, 2019.

495   Bolton, W. R., Hinzman, L., and Yoshikawa, K.: Water balance dynamics of three small catchments in a Sub-Arctic boreal forest, IAHS-AISH Publication, 290, 213–223, 2004.

Bonanza Creek LTER: Study Sites & Design: Caribou-Poker Creeks Research Watershed, https://www.lter.uaf.edu/research/study-sites-cpcrw, last access: 29 October 2024.
500
Bredthauer, S. R., and Hoch, D.: Drainage network analysis of a subarctic watershed, Caribou-Poker Creeks research watershed, interior Alaska, US Cold Regions Research and Engineering Laboratory Hanover, NH, Special Report, 79-l9, 1979.

505   Brown, R. D., and Goodison, B. E.: Interannual variability in reconstructed Canadian snow cover, 1915-1992, J. Climate, 9(6), 1299–1318, https://doi.org/10.1175/1520-0442(1996)009<1299:IVIRCS>2.0.CO;2, 1996.

Broxton, P. D., Harpold, A. A., Biederman, J. A., Troch, P. A., Molotch, N. P., and Brooks, P. D.: Quantifying the effects of vegetation structure on snow accumulation and ablation in mixed-conifer forests, Ecohydrology, 8(6), 1073–1094,
510   https://doi.org/10.1002/eco.1565, 2015.

Broxton, P. D., van Leeuwen, W. J. D., and Biederman, J. A.: Improving Snow Water Equivalent Maps With Machine Learning of Snow Survey and Lidar Measurements, Water Resour. Res., 55(5), 3739–3757,
https://doi.org/10.1029/2018WR024146, 2019.
515

Campbell, M. J., Dennison, P. E., Hudak, A. T., Parham, L. M., and Butler, B. W.: Quantifying understory vegetation density using small-footprint airborne lidar. Remote Sens. Environ., 215, 330-342, https://doi.org/10.1016/j.rse.2018.06.023,
2018.

520   Carroll, S. S., and Cressie, N.: A comparison of geostatistical methodologies used to estimate snow water equivalent, Water Resour. Bull., 32(2), 267–278, https://doi.org/10.1111/j.1752-1688.1996.tb03450.x, 1996.

Chapin, F. S., Mcguire, A. D., Randerson, J., Pielke, R., Baldocchi, D., Hobbie, S. E., Roulet, N., Eugster, W., Kasischke, E., Rastetter, E. B., Zimov, S. A., and Running, S. W.: Arctic and boreal ecosystems of western North America as components
525   of the climate system, Global Change Biol., 6(1), 211–223, https://doi.org/10.1046/j.1365-2486.2000.06022.x, 2000.

Chapin, F. S., Sturm, M., Serreze, M. C., McFadden, J. P., Key, J. R., Lloyd, A. H., McGuire, A. D., Rupp, T. S., Lynch, A. H., Schimel, J. P., Beringer, J., Chapman, W. L., Epstein, H. E., Euskirchen, E. S., Hinzman, L. D., Jia, G., Ping, C. L., Tape, K. D., Thompson, C. D. C., Welker, J. M.: Role of land-surface changes in arctic summer warming, Science, 310(5748),
530   657–660, https://doi.org/10.1126/science.1117368, 2005.

Cho, E., Hunsaker, A. G., Jacobs, J. M., Palace, M., Sullivan, F. B., and Burakowski, E. A.: Maximum entropy modeling to identify physical drivers of shallow snowpack heterogeneity using unpiloted aerial system (UAS) lidar, J. Hydrology, 602, 126722, https://doi.org/10.1016/j.jhydrol.2021.126722, 2021.
535

Contreras, M. A., Staats, W., Yiang, J., and Parrott, D.: Quantifying the accuracy of LiDAR-derived DEM in deciduous eastern forests of the Cumberland Plateau, J. Geo. Info. System, 9(3), 339-353, https://doi.org/10.4236/jgis.2017.93021,
2017.

540 Currier W.R., Pflug J., Mazzotti G., Jonas T., Deems J.S., Bormann K.J., Painter T.H., Hiemstra C.A., Gelvin A., Uhlmann Z., and Spaete L.: Comparing aerial lidar observations with terrestrial lidar and snow-probe transects from NASA's 2017 SnowEx campaign, Water Resour. Res., 55(7), 6285-6294, https://doi.org/10.1029/2018wr024533, 2019.

Deems, J. S., Painter, T. H., and Finnegan, D. C.: Lidar measurement of snow depth: a review. J. Glaciol., 59(215), 467-479,
545 https://doi.org/10.3189/2013JoG12J154, 2013.

Dewitz, J.: National Land Cover Database (NLCD) 2016 Products (ver. 3.0, November 2023), U.S. Geological Survey, https://Doi.Org/10.5066/P96HHBIE, 2019.

550 Dharmadasa, V., Kinnard, C., and Baraër, M.: An Accuracy Assessment of Snow Depth Measurements in Agro-Forested Environments by UAV Lidar, Remote Sens., 14(7), 1649, https://doi.org/10.3390/rs14071649, 2022.

Dickerson-Lange, S. E., Vano, J. A., Gersonde, R., and Lundquist, J. D.: Ranking Forest Effects on Snow Storage: A Decision Tool for Forest Management, Water Resour. Res., 57(10), e2020WR027926,
555 https://doi.org/10.1029/2020WR027926, 2021.

Diez, D. M., and Barr, C. D.: OpenIntro Statistics, 2nd ed., Boston, MA, USA, https://www.openintro.org/book/os/, 2012.
Douglas, T. A., and Zhang, C.: Machine learning analyses of remote sensing measurements establish strong relationships between vegetation and snow depth in the boreal forest of Interior Alaska, Environ. Res. Lett., 16(6), 065014,
560 https://doi.org/10.1088/1748-9326/ac04d8, 2021.

Erxleben, J., Elder, K., and Davis, R.: Comparison of spatial interpolation methods for estimating snow distribution in the Colorado Rocky Mountains, Hydrol. Process., 16(18), 3627–3649, https://doi.org/10.1002/hyp.1239, 2002.

565 Gould, S. B., Glenn, N. F., Sankey, T. T., and McNamara, J. P.: Influence of a dense, low-height shrub species on the accuracy of a LiDAR-derived DEM, Photo. Eng. Remote Sens., 79(5), 421-431, https://doi.org/10.14358/PERS.79.5.421, 2013.

Güntner, A., Stuck, J., Werth, S., Döll, P., Verzano, K., and Merz, B.: A global analysis of temporal and spatial variations in
570 continental water storage, Water Resour. Res., 43(5), W05416, https://doi.org/10.1029/2006WR005247, 2007.

Harpold, A. A., Guo, Q., Molotch, N., Brooks, P. D., Bales, R., Fernandez-Diaz, J. C., Musselman, K. N., Swetnam, T. L., Kirchner, P., Meadows, M. W., Flanagan, J., and Lucas, R.: LiDAR-derived snowpack data sets from mixed conifer forests across the Western United States, Water Resour. Res., 50(3), 2749–2755, https://doi.org/10.1002/2013WR013935, 2014.

575

Haugen, R. K., Slaughter, C. W., Howe, K. E., and Dingman, S. L.: Hydrology and climatology of the Caribou-Poker creeks research watershed, Alaska, US Army Cold Regions Research and Engineering Laboratory CRREL, Report 82-26, Hanover, NH, USA, 1982.

580   Hojatimalekshah, A., Uhlmann, Z., Glenn, N. F., Hiemstra, C. A., Tennant, C. J., Graham, J. D., Spaete, L., Gelvin, A., Marshall, H. P., McNamara, J. P., and Enterkine, J.: Tree canopy and snow depth relationships at fine scales with terrestrial laser scanning, Cryosphere, 15(5), 2187–2209, https://doi.org/10.5194/tc-15-2187-2021, 2021.

Homan, J. W., and Kane, D. L.: Arctic snow distribution patterns at the watershed scale, Hydrol. Res., 46(4), 507–520,
585   https://doi.org/10.2166/nh.2014.024, 2015.

Hopkinson, C., Collins, T., Anderson, A., Pomeroy, J., and Spooner, I.: Spatial snow depth assessment using LiDAR transect samples and public GIS data layers in the Elbow River Watershed, Alberta, Water Resour. J., 37(2), 69–87, https://doi.org/10.4296/cwrj3702893, 2012.

590

Hopkinson, C., Sitar, M., Chasmer, L., and Treitz, P.: Mapping snowpack depth beneath forest canopies using airborne lidar, Photogramm. Eng. Rem. S., 70(3), 323–330, https://doi.org/10.14358/PERS.70.3.323, 2004.

Huang, C. L., Wang, H. W., and Hou, J. L.: Estimating spatial distribution of daily snow depth with kriging methods:
595   combination of MODIS snow cover area data and ground-based observations, Cryosphere Discussions, 9(5), 4997–5020, doi:10.5194/tcd-9-4997-2015, 2015.

Jacobs, J. M., Hunsaker, A. G., Sullivan, F. B., Palace, M., Burakowski, E. A., Herrick, C., and Cho, E.: Snow depth mapping with unpiloted aerial system lidar observations: A case study in Durham, New Hampshire, United States,
600   Cryosphere, 15(3), 1485–1500, https://doi.org/10.5194/tc-15-1485-2021, 2021.

Kane, D. L., and Yang, D.: Overview of water balance determinations for high latitude watersheds, IAHS-AISH Publications-Series of Proceedings and Reports, 290, 1–12, 2004.

605   Koutantou, K., Mazzotti, G., Brunner, P., Webster, C., & Jonas, T.: Exploring snow distribution dynamics in steep forested slopes with UAV-borne LiDAR, Cold Reg. Sci. Technol., 200 (5), 103587, https://doi.org/10.1016/j.coldregions.2022.103587, 2022.

        Kozii, N., Laudon, H., Ottosson-Löfvenius, M., and Hasselquist, N. J.: Increasing water losses from snow captured in the
610   canopy of boreal forests: A case study using a 30 year data set, Hydrol. Process., 31(20), 3558–3567, https://doi.org/10.1002/hyp.11277, 2017.

        Kruskal, W. H., and Wallis, W. A.: Use of Ranks in One-Criterion Variance Analysis, J. Am. Stat. Assoc., 47(260), 583–621, https://doi.org/10.1080/01621459.1952.10483441, 1985.
615

        Lader, R., Walsh, J. E., Bhatt, U. S., and Bieniek, P. A.: Anticipated changes to the snow season in Alaska: Elevation dependency, timing and extremes, Int. J. Climatol., 40(1), 169–187, https://doi.org/10.1002/joc.6201, 2020.

        Larsen, C.: SnowEx23 Airborne Lidar-Derived 0.25M Snow Depth and Canopy Height, (SNEX23_Lidar, Version 1) [Data
620   Set], Boulder, Colorado, USA, NASA National Snow and Ice Data Center Distributed Active Archive Center, https://doi.org/10.5067/BV4D8RRU1H7U, 2024.

        Li, J., Larsen, C., Rodriguez-Morales, F., Arnold, E., Leuschen, C., Paden, J., Shang, J., and Gomez-Garcia, D.: Comparison of coincident forest canopy measurements from airborne lidar and ultra-wideband microwave radar, Int. Geosci. Remote Se.
625   (IGARSS), Brussels, Belgium, 12 October 2012, https://doi.org/10.1109/IGARSS47720.2021.9554932, 2021.

        Liston, G. E., and Hiemstra, C. A.: The changing cryosphere: Pan-Arctic snow trends (1979-2009), J. Climate, 24(21), 5691–5712, https://doi.org/10.1175/JCLI-D-11-00081.1, 2011.

630   Liston, G. E., and Sturm, M.: A snow-transport model for complex terrain, J. Glaciol., 44(148), 498–516, https://doi.org/10.1017/S0022143000002021, 1998.

        Lloyd, C. D., and Atkinson, P. M.: Assessing uncertainty in estimates with ordinary and indicator kriging, Comput. Geosci., 27(8), 929–937, https://doi.org/10.1016/S0098-3004(00)00132-1, 2001.
635

        Lundquist, J. D., Dickerson-Lange, S. E., Lutz, J. A., and Cristea, N. C.: Lower forest density enhances snow retention in regions with warmer winters: A global framework developed from plot-scale observations and modeling, Water Resour. Res., 49(10), 6356–6370, https://doi.org/10.1002/wrcr.20504, 2013.

640   MacGregor, J. A., Boisvert, L. N., Medley, B., Petty, A. A., Harbeck, J. P., Bell, R. E., Blair, J. B., Blanchard-
       Wrigglesworth, E., Buckley, E. M., Christoffersen, M. S., Cochran, J. R., Csathó, B. M., De Marco, E. L., Dominguez, R. A.
       T., Fahnestock, M. A., Farrell, S. L., Gogineni, S. P., Greenbaum, J. S., Hansen, C. M., and Yungel, J. K.: The Scientific
       Legacy of NASA's Operation IceBridge, Rev. Geophys., 59(2), e2020RG000712, https://doi.org/10.1029/2020RG000712,
       2021.

645

       Mann, H. B., and Whitney, D. R.: On a Test of Whether one of Two Random Variables is Stochastically Larger than the
       Other, Ann. Math. Stat., 18(1), 50–60, https://doi.org/10.1214/aoms/1177730491, 1947.

       May, L., Stuefer, S., Vuyovich, C. M., Elder, K., Osmanoglu, B., Marshall, H., Durand, M., Vas, D., Gelvin, A. B., Liddle
650   Broberg, K. and Maakestad, J.: SnowEx23 Mar22 IOP Snow Depth Measurements, (SNEX23_MAR22_SD, Version 1)
       [Data Set], Boulder, Colorado, USA, NASA National Snow and Ice Data Center Distributed Active Archive Center,
       https://doi.org/10.5067/086OMZDJP2W6, 2024.
       Mazzotti, G., Currier, W. R., Deems, J. S., Pflug, J. M., Lundquist, J. D., and Jonas, T.: Revisiting Snow Cover Variability
       and Canopy Structure Within Forest Stands: Insights From Airborne Lidar Data, Water Resour. Res., 55(7)., 6198–6216,
655   https://doi.org/10.1029/2019WR024898, 2019.

       Moeser, D., Mazzotti, G., Helbig, N., and Jonas, T.: Representing spatial variability of forest snow: Implementation of a new
       interception model, Water Resour. Res., 52(2), 1208–1226, https://doi.org/10.1002/2015WR017961, 2016.

660   Nolan, M., Larsen, C., and Sturm, M.: Mapping snow depth from manned aircraft on landscape scales at centimeter
       resolution using structure-from-motion photogrammetry, Cryosphere, 9(4), 1445–1463, https://doi.org/10.5194/tc-9-1445-
       2015, 2015.

       Ohmer, M., Liesch, T., Goeppert, N., and Goldscheider, N.: On the optimal selection of interpolation methods for
665   groundwater contouring: An example of propagation of uncertainty regarding inter-aquifer exchange, Adv. Water Resour.,
       109, 121–132, https://doi.org/10.1016/j.advwatres.2017.08.016, 2017.

       Painter, T. H., Berisford, D. F., Boardman, J. W., Bormann, K. J., Deems, J. S., Gehrke, F., Hedrick, A., Joyce, M., Laidlaw,
       R., Marks, D., Mattmann, C., McGurk, B., Ramirez, P., Richardson, M., Skiles, S. M. K., Seidel, F. C., and Winstral, A.:
670   The Airborne Snow Observatory: Fusion of scanning lidar, imaging spectrometer, and physically-based modeling for
       mapping snow water equivalent and snow albedo, Remote Sens. Environ., 184, 139–152,
       https://doi.org/10.1016/j.rse.2016.06.018, 2016.

Panda, S. K., Prakash, A., Solie, D. N., Romanovsky, V. E., and Jorgenson, M. T.: Remote sensing and field-based mapping
675   of permafrost distribution along the Alaska Highway corridor, interior Alaska, Permafrost Periglac., 21(3), 271–281,
https://doi.org/10.1002/ppp.686, 2010.

Pastick, N. J., Jorgenson, M. T., Wylie, B. K., Nield, S. J., Johnson, K. D., and Finley, A. O.: Distribution of near-surface
permafrost in Alaska: Estimates of present and future conditions, Remote Sens. Environ., 168, 301–315,
680   https://doi.org/10.1016/j.rse.2015.07.019, 2015.

Pomeroy, J. W., Gray, D. M., Hedstrom, N. R., and Janowicz, J. R.: Prediction of seasonal snow accumulation in cold
climate forests, Hydrol. Process., 16(18), 3543–3558, https://doi.org/10.1002/hyp.1228, 2002.

685   R Core Team.: *R*: A Language and Environment for Statistical Computing, https://www.R-project.org/, R Foundation for
Statistical Computing, 2022, last access:18 September 2024.
Reinking, A. K., Pedersen, S.H., Elder, K., Boelman, N. T., Glass, T. W., Oates, B. A., Bergen, S., Coughenour, M.B., Feltner,
J.A., Barker, K.J., Prugh, L.R., Brinkman, T.J., Bentzen, T.W., Pedersen, A.O., Schmidt, N.M., and Liston, G. E.:
Collaborative wildlife–snow science: Integrating wildlife and snow expertise to improve research and
690   management. Ecosphere, 13(6), e4094, https://doi.org/10.1002/ecs2.4094, 2022.

Reutebuch, S. E., Mc Gaughey, R. J., Andersen, H. E., and Carson, W. W.: Accuracy of a high-resolution lidar terrain model
under a conifer forest canopy, Can. J. Remote Sens., 29(5), 527–535, https://doi.org/10.5589/m03-022, 2003.

695   Siirila-Woodburn, E.R., Rhoades, A.M., Hatchett, B.J., Huning, L.S., Szinai, J., Tague, C., Nico, P.S., Feldman, D.R., Jones,
A.D., Collins, W.D. and Kaatz, L.: A low-to-no snow future and its impacts on water resources in the western United
States. Nat Rev Earth Environ **2**, 800–819, https://doi.org/10.1038/s43017-021-00219-y, 2021.

Smith, C. W., Panda, S. K., Bhatt, U. S., and Meyer, F. J.: Improved boreal forest wildfire fuel type mapping in interior
700   alaska using aviris-ng hyperspectral data, Remote Sens., 13(5), 897, https://doi.org/10.3390/rs13050897, 2021.

Spaete, L. P., Glenn, N. F., Derryberry, D. R., Sankey, T. T., Mitchell, J. J., and Hardegree, S. P.: Vegetation and slope
effects on accuracy of a LiDAR-derived DEM in the sagebrush steppe. Remote Sens. Lett., 2(4), 317-326,
https://doi.org/10.1080/01431161.2010.515267, 2011.
705

Stuefer, S., Kane, D. L., and Liston, G. E.: In situ snow water equivalent observations in the US Arctic. Hydrol. Res., 44(1), 21-34, 2013.

Storck, P., Lettenmaier, D. P., and Bolton, S. M.: Measurement of snow interception and canopy effects on snow
710 accumulation and melt in a mountainous maritime climate, Oregon, United States, Water Resour. Res., 38(11), 5-1, https://doi.org/10.1029/2002wr001281, 2002.

Sturm, M., and Holmgren, J.: An Automatic Snow Depth Probe for Field Validation Campaigns, Water Resour. Res., 54(11), 9695–9701, https://doi.org/10.1029/2018WR023559, 2018.
715
Sturm, M., and Liston, G. E.: Revisiting the Global Seasonal Snow Classification: An Updated Dataset for Earth System Applications, J. Hydrometeorol., 22(11), 2917–2938, https://doi.org/10.1175/jhm-d-21-0070.1, 2021.

Tabari, H., Marofi, S., Abyaneh, H. Z., and Sharifi, M. R.: Comparison of artificial neural network and combined models in
720 estimating spatial distribution of snow depth and snow water equivalent in Samsami basin of Iran, Neural Comput. Appl., 19(4), 625–635, https://doi.org/10.1007/s00521-009-0320-9, 2010.

Tennant, C. J., Harpold, A. A., Lohse, K. A., Godsey, S. E., Crosby, B. T., Larsen, L. G., Brooks, P. D., Van Kirk, R. W., and Glenn, N. F.: Regional sensitivities of seasonal snowpack to elevation, aspect, and vegetation cover in western North
725 America, Water Resour. Res., 53(8), 6908–6926, https://doi.org/10.1002/2016WR019374, 2017.

Tinkham, W. T., Smith, A. M. S., Marshall, H. P., Link, T. E., Falkowski, M. J., and Winstral, A. H.: Quantifying spatial distribution of snow depth errors from LiDAR using Random Forest, Remote Sens. Environ., 141, 105–115, https://doi.org/10.1016/j.rse.2013.10.021, 2014.
730
Trujillo, E., Ramírez, J. A., and Elder, K. J.: Topographic, meteorologic, and canopy controls on the scaling characteristics of the spatial distribution of snow depth fields, Water Resour. Res., 43(7), W07409, https://doi.org/10.1029/2006WR005317, 2007.

735 Uhlmann, Z., Glenn, N. F., Spaete, L. P., Hiemstra, C., Tennant, C., and McNamara, J.: Resolving the influence of forest-canopy structure on snow depth distributions with terrestrial laser scanning, Int. Geosci. Remote Se. (IGARSS), July 2018, https://doi.org/10.1109/IGARSS.2018.8517911, 2018.

USDA Forest Service Pacific Northwest Research Station.: Bonanza Creek Experimental Forest and Caribou-Poker Creeks
740   Research Watershed, 2 May 2023, https://research.fs.usda.gov/pnw/forestsandranges/locations/bcef-cpcrw, last access: 30
October 2024.

USDA Natural Resources Conservation Service: https://www.nrcs.usda.gov/, last access: 30 October 2024.

745   Vuyovich, C., Stuefer S., Durand, M., Marshall, H. P., Osmanogln, B., Elder, K., Vas, D., Gelvin, A., Larsen, C., Pedersen,
S., Hodkinson, D., Deeb, E., Mason, M., and Youcha, E.: NASA SnowEx 2023 Experiment Plan, June 2024,
https://snow.nasa.gov/campaigns/snowex-2023-tundra-and-boreal-forest, 2024.

Webb, R. W., Raleigh, M. S., McGrath, D., Molotch, N. P., Elder, K., Hiemstra, C., Brucker, L., and Marshall, H. P.:
750   Within-Stand Boundary Effects on Snow Water Equivalent Distribution in Forested Areas, Water Resour. Res., 56(10),
e2019WR024905, https://doi.org/10.1029/2019WR024905, 2020.

Woo, M. K.: Moisture and Heat, in: Permafrost Hydrology, Springer-Verlag, Berlin, Heidelberg, Germany, 35–72,
https://doi.org/10.1007/978-3-642-23462-0, 2012.
755
Yang, L., Jin, S., Danielson, P., Homer, C., Gass, L., Bender, S. M., Case, A., Costello, C., Dewitz, J., Fry, J., Funk, M.,
Granneman, B., Liknes, G. C., Rigge, M., and Xian, G.: A new generation of the United States National Land Cover
Database: Requirements, research priorities, design, and implementation strategies, ISPRS J. Photogramm., 146, 108–123,
https://doi.org/10.1016/j.isprsjprs.2018.09.006, 2018.
760
Zheng, Z., Kirchner, P. B., and Bales, R. C.: Topographic and vegetation effects on snow accumulation in the southern
Sierra Nevada: A statistical summary from lidar data, Cryosphere, 10(1), 257–269, https://doi.org/10.5194/tc-10-257-2016,
2016.